VON MOLTKE, T., PISTORIUS, P.C., and SANDENBERGH, R.F. The influence of heat-tinted surface layers on the corrosion resistance of stainless steels. *INFACON 6. Proceedings of the 1st International Chromium Steel and Alloys Congress, Cape Town.* Volume 2. Johannesburg, SAIMM, 1992. pp. 185–195.

The Influence of Heat-tinted Surface Layers on the Corrosion Resistance of Stainless Steels

T. VON MOLTKE*, P.C. PISTORIUS†, and R.F. SANDENBERGH†

**Iscor Ltd, South Africa*

†University of Pretoria, Pretoria, South Africa

The composition of heat-tinted layers formed on type 304 stainless steel during welding and on simulated weld specimens was analysed by Auger electron spectroscopy. The low-temperature oxides are iron-rich, those formed at intermediate temperatures are chromium-rich, and those formed at the highest temperatures (ca 1000 °C and above) are depleted in chromium probably owing to the volatilization of chromium trioxide.

The pitting potentials of the simulated specimens (in 3,5 per cent NaCl at pH 1) followed the chromium content of the outer oxide film: those films with a low chromium content (formed in the range 400 to 600 °C) had the most cathodic pitting potentials. The low pitting potentials are associated with a large increase in the surface density of the pits, and a reduction in the average size to which the metastable pits grow before repassivating. The iron-rich oxide film dissolves in the acidic solution used here, with the result that a deleterious effect is observed only if the potential moves rapidly into the pitting range. The colour of the heat-tinted surface does not serve as an indication of either the composition of the oxide or of its resistance to pitting.

Introduction

During the welding of stainless steels, the metal adjacent to the weld is oxidized. In those regions of the metal heated to about 400 °C or greater[1], the thermal oxide layer causes visible discoloration of the metal surface – the metal is 'heat tinted'. Heat tint is sometimes implicated in service failures by pitting corrosion. It is possible that the deleterious effect of heat tint can be understood from an examination of the effect of thermal oxidation on the two paradoxical roles of the oxide film: as a barrier to corrosion (and pit initiation), and in stabilizing pits once they have formed.

The good corrosion resistance of stainless steel is imparted by the passive film, which forms a kinetic barrier to corrosion. However, under conditions conducive to pitting corrosion (most commonly in chloride-containing environments), this passive film has a paradoxical role – the early growth stage of pits ('metastable' growth[2]) is stabilized by the passive film, which forms a cover over the mouth of the growing pit[3]. This cover acts as a barrier to diffusion, and so aids the maintenance of an aggressive anolyte inside the pit. This anolyte must have a very high concentration of chloride ions and a low pH to sustain rapid dissolution of the metal; for type 304 stainless steel, the concentration of the metal cations (produced by dissolution) must be at least 75 per cent of the saturation concentration of the metal chloride[4]. The effect of the oxide film in stabilizing pit growth has been demonstrated by Isaacs and Kissel[5], who found enhanced pit lifetimes on the surfaces of type 304 stainless steel that had been oxidized in air in the range 110 to 300 °C.

The composition of passive films formed at room temperature has been shown to affect pit nucleation (as measured by the pitting potential): a positive correlation was found between the pitting potential and the chromium content of the passive film[6]. (It should be noted that the different chromium concentrations were achieved through various passivation treatments with solutions containing nitric acid or mixtures of hydrofluoric and nitric acid; these treatments may also dissolve out the sulphides that can act as pit-initiation sites. Thus, the observation of a correlation between the chromium content and the pitting potential does not unambiguously demonstrate a direct role for the composition of the oxide film in the pit-nucleation process.) In the case of an 18 per cent ferritic stainless steel, which had been thermally oxidized in the range 300 to 475 °C at low oxygen partial pressures (10^{-11} to 10^{-8} torr), a positive correlation between the relative chromium content of the oxide film and the resistance to crevice corrosion was also found[7]. From these results, it appears likely that the composition of the oxide film affects the initiation of localized corrosion.

This paper concerns the pitting-corrosion behaviour of heat-tinted type 304 stainless steel, and the relative importance of the two opposite roles of the oxide film: limiting pit initiation, and stabilizing pit growth.

Experimental Method

Type 304 stainless-steel sheet of 1 mm thickness was tested. The composition of the steel is given in Table I. An autogenous tungsten inert-gas (TIG) weld was put on some

plate specimens after a gold layer approximately 15 nm thick had been sputtered onto the metal surface. This gold layer served as a marker during subsequent Auger analysis. The fused zone of the autogenous weld was approximately 3 mm wide on the welded side, and extended through the thickness of the plate.

TABLE I
COMPOSITION OF THE TYPE 304 STAINLESS STEEL USED IN THIS WORK IN WT PER CENT

C	Mn	P	S	Si	Ni	Cu	Cr	Mo	V	Al
0,05	1,54	0,029	0,010	0,19	8,6	0,065	17,82	0,035	0,10	0,026

Other specimens were oxidized in air by means of a weld simulator, which heats the specimens by electrical resistance heating. The specimens were 18 mm wide, with a length of 28 mm between the water-cooled copper clamps that served as current contacts. The temperature at the centre of each specimen was monitored by means of a Pt–13%Rh/Pt (R-type) thermocouple. The specimens were heated rapidly to the peak temperature and, after being held at that temperature, were allowed to cool by conduction to the water-cooled clamps, and radiation and convection to the environment. This gave a cooling time from 800 to 500 °C of approximately 10 seconds. This is illustrated by Figure 1, which shows the thermal history of a specimen that was heated to 880 °C. Specimens were heated to peak temperatures from 280 to 980 °C, and each specimen was

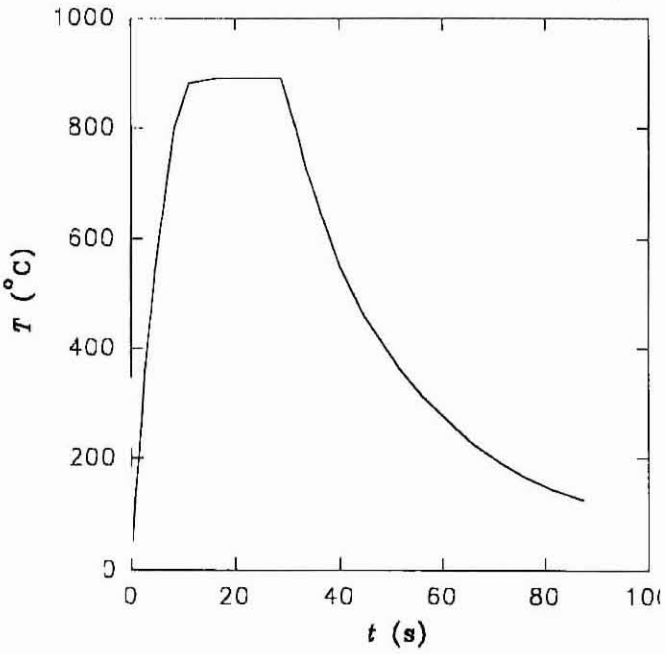

FIGURE 1. Heating cycle of specimen heated to 880 °C in the weld simulator

exposed to a single heating cycle. The surface preparation before heating consisted of wet abrasion to a 600 grit finish, and passivation in 20 per cent HNO_3 at 60 °C for 30 minutes.

The compositions of the surface films on the welded and simulated specimens were determined by Auger electron spectroscopy, using a Perkin-Elmer PHI 600 scanning Auger microprobe.

Potentiodynamic tests were performed in 3,5 per cent NaCl adjusted to pH 1 with HCl. The simulated specimens were tested in this solution at the ambient temperature of 24±2 °C. Welded specimens were tested potentiodynamically at 60 °C; some weld specimens were also immersed in this solution under open-circuit conditions for periods of up to 12 days. All the solutions were stagnant and were not deaerated. The potential scans started at the corrosion potential after exposure of the specimens to the test solution for 5 minutes. A sweep rate of 1 mV/s was used for the simulated specimens, and 0,1 and 5 mV/s for the weld specimens. Experiments were terminated when the current exceeded 40 μA, indicating the presence of a stably growing pit. The exposed area of the specimen was 1,2 cm^2

The potential profile over a freely corroding welded specimen immersed in a solution of 10 per cent $FeCl_3$ was determined with a scanning reference electrode (SRET[8]). A tin electrode[9] with an outer diameter of 50 μm was placed 50 μm above the surface of the welded specimen, and scanned paralled to this surface by means of stepper motors. The potential profile was read into a personal computer with an analogue-to-digital (A/D) converter card. The potential of the tin electrode was about -400 mV relative to a silver–silver chloride electrode. With the exception of the SRET results, all the potentials in this paper are quoted relative to the silver–silver chloride electrode.

Results

Simulated Specimens

The specimens heated in the weld simulator developed tints that are visually similar to those observed adjacent to welds. Those specimens exposed to a peak temperature of 280 °C developed a faint straw colour; this colour deepened with increasing temperature. Specimens heated to between 600 and 900 °C developed a blue tint, while those with a peak temperature of 980 °C showed a brownish tint. These colours result mainly from different film thicknesses, and do not serve as an indication of the composition of the oxide film. This is illustrated by Figure 2, which gives the composition of the outer layer of the oxide film as a function of the peak temperature. The graph plots the chromium content of the outer oxide film relative to the total iron and chromium concentrations (atomic percentages). It is apparent from Figure 2 that the temperature range 600 to 900 °C is associated with significant changes in film composition, while it was observed that the colour of the oxide is largely

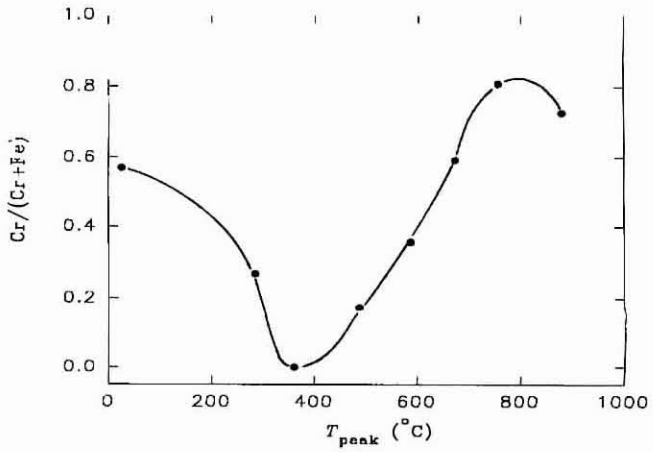

FIGURE 2. Relative chromium content of the outer oxide films on specimens heated to different peak temperatures for 20 seconds

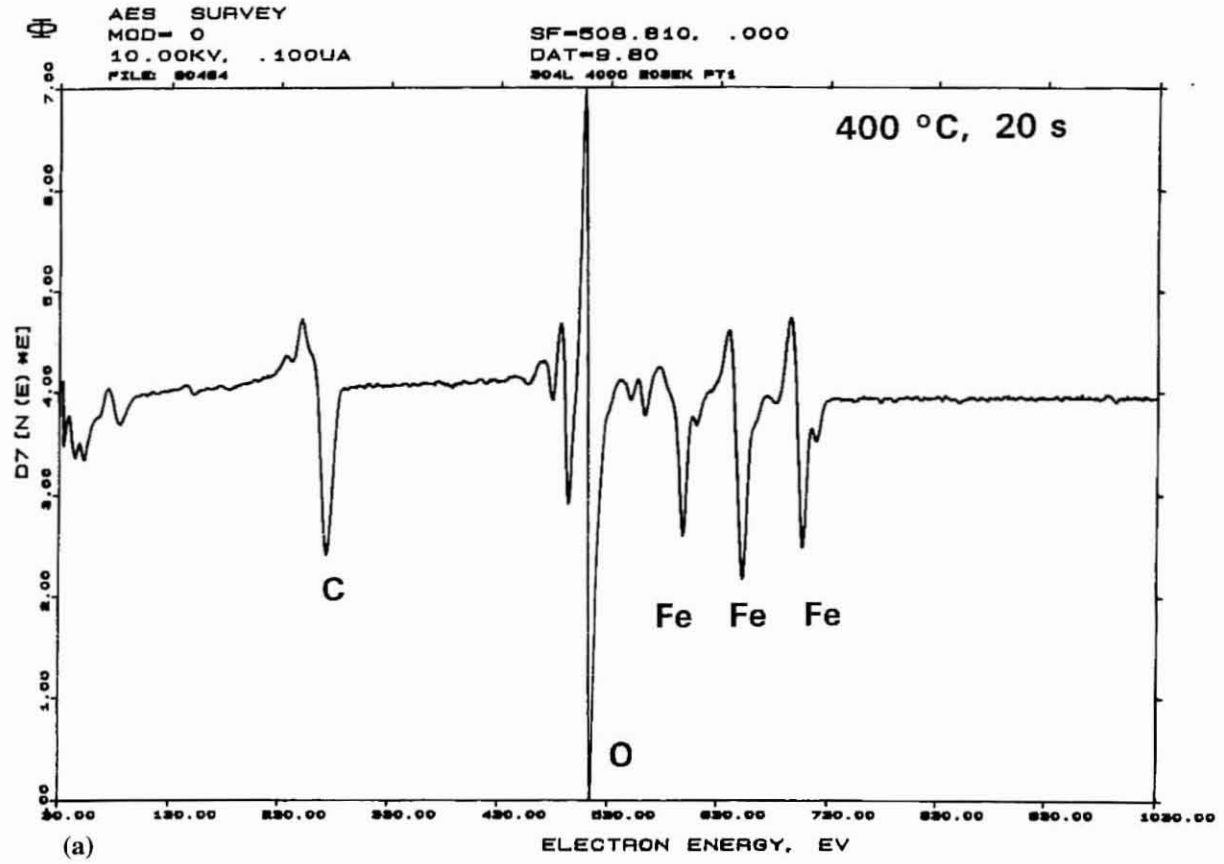

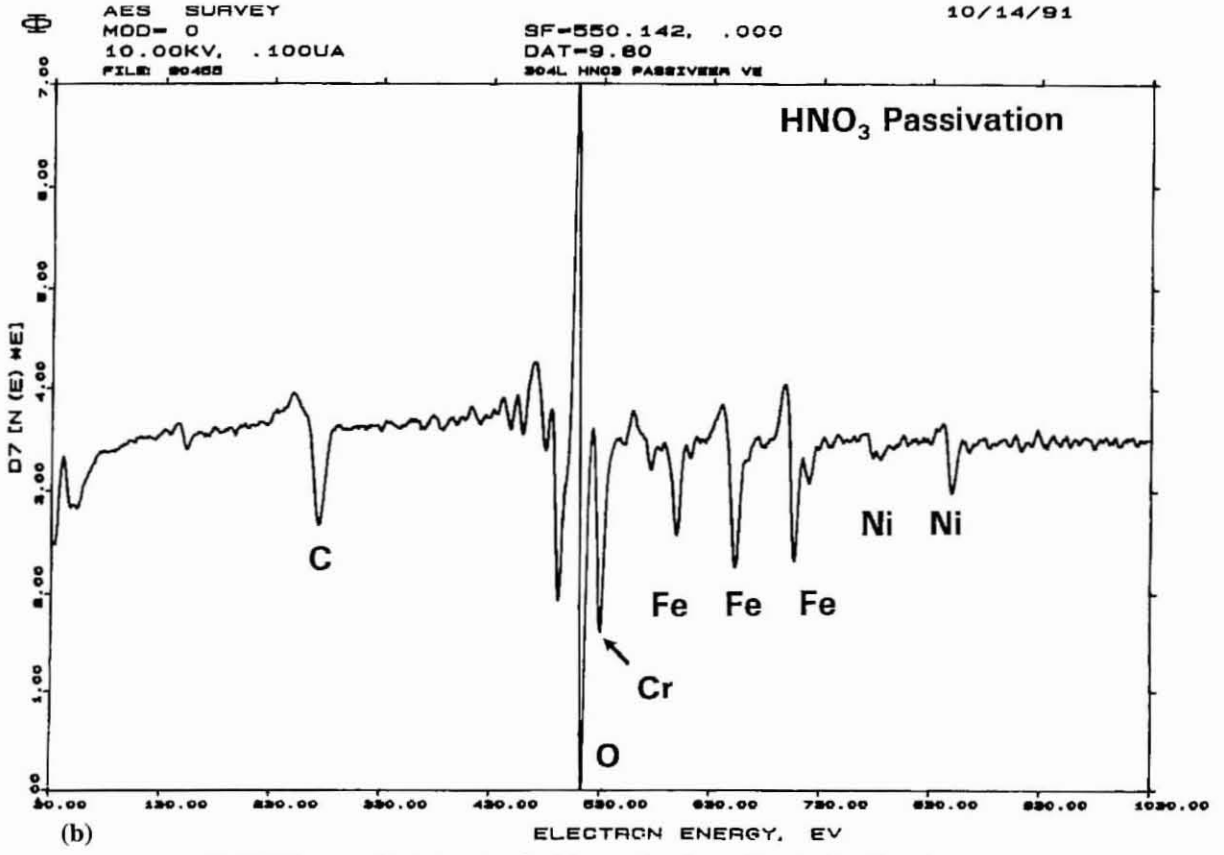

FIGURE 3. Auger-electron spectra of stainless-steel surfaces with and without heat tint
(a) Specimen heated to 380 °C, showing the absence of chromium in the outer oxide
(b) Passivated specimen

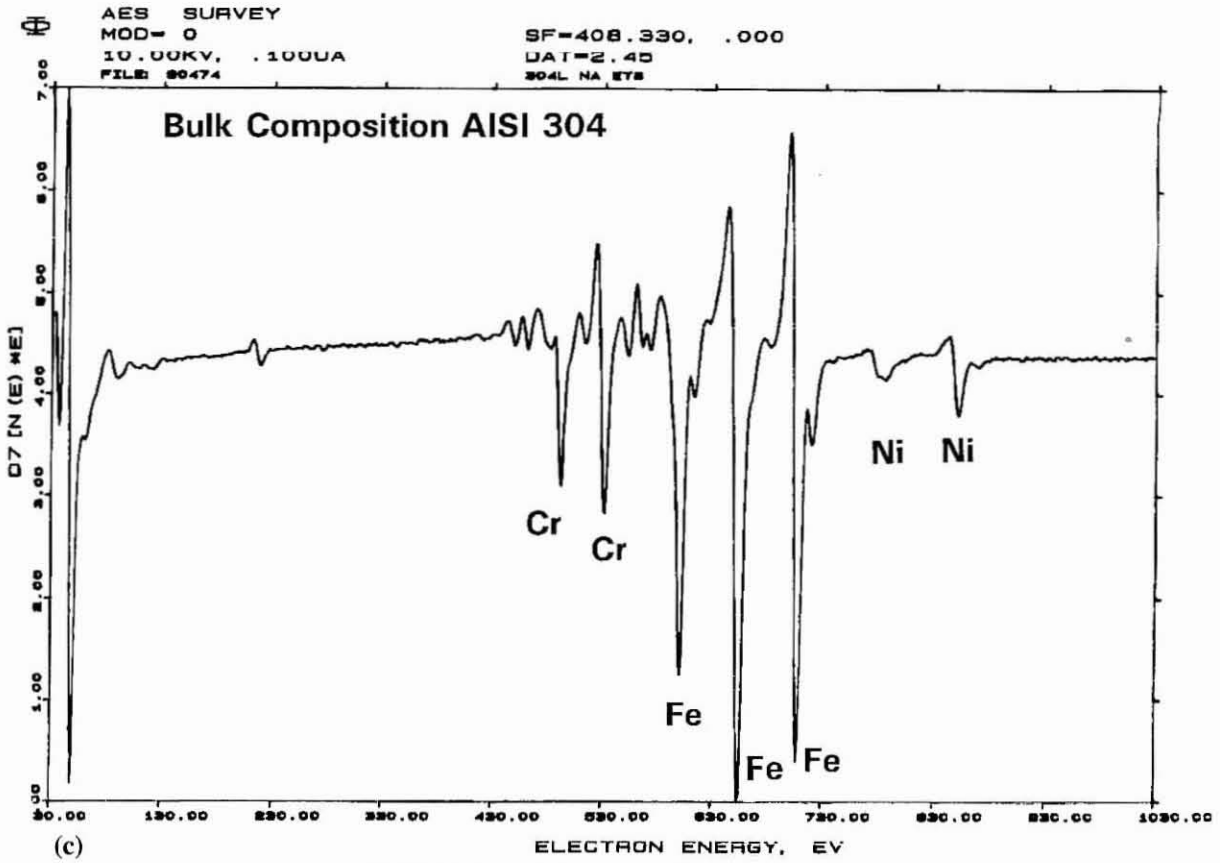

FIGURE 4. Auger-electron spectra of bulk metal

unaffected. The data point at 25 °C in Figure 2 refers to a specimen that was only passivated and was not subsequently air-oxidized.

Figure 2 reveals a strong effect of the peak temperature on the the composition of the outer film. The film on the passivated specimen is enriched in chromium: the atomic ratio of chromium to iron in the film is 1,3 while the bulk ratio is 0,27. This chromium enrichment is in line with the findings of others[6,10]. The outer surface of oxides formed in the temperature range 280 to 580 °C contains predominantly iron. This is exemplified by the Auger electron spectrum in Figure 3(a), which shows no trace of chromium in the outer surface of an oxide formed at 380 °C. This effect is especially striking if this spectrum is compared with those for the passivated specimen, Figure 3(b), and for a specimen that had been sputtered down to the base metal, Figure 4.

At temperatures above 480 to 880 °C, chromium was also detected in the outer film; at the upper end of this range, chromium predominates over iron. Depth profiles show that, at the lower temperatures where the outer surface is enriched in iron, chromium is present in the film below the iron-rich surface, Figure 5(a). Figure 5(b) shows a depth profile for a chromium-rich oxide film. It appears that the temperature of oxidation has an effect on the relative magnitudes of the diffusion coefficients of iron and chromium. At lower temperatures, the diffusion coefficient of iron is greater, while chromium diffuses faster at higher temperatures.

Figure 2 also shows that the chromium content of the outer film again decreases at the upper end of the temperature range considered here. This effect is probably due to the loss of chromium[11] as the volatile oxide CrO_3.

The pitting corrosion of the simulated specimens changes in tandem with the changes in film composition (Figure 6). This figure gives the breakdown potential as a function of the peak temperature. A comparison of Figure 2 and Figure 6 shows that large decreases (of up to 200 mV) in the pitting potential are associated with those temperature ranges in which the outer film is iron-rich. These changes in the breakdown potential are caused by the surface condition of the metal, and not by any internal changes (such as sensitization). This was demonstrated by the breakdown potentials of specimens that had been exposed to peak temperatures of 380 °C and 755 °C, and had then had the oxide film removed by grinding. The breakdown potential was within 10 mV of 700 mV (silver–silver chloride) in both cases, which is the same as for the specimen that had not been oxidized at all at elevated temperatures.

The change in pitting potential is accompanied by an altered pit morphology and surface density. Figure 7 shows the appearance, after the pitting test in 3,5 per cent NaCl, of the surfaces of a passivated specimen, and of specimens oxidized at 380 and 880 °C respectively. It should be noted that the pits visible in Figure 7 are metastable pits. These pits could be observed visually on the surface of the specimen before the breakdown potential was reached. Figure 7(b) reveals that the specimen oxidized at 380 °C has a much greater surface density of metastable pits compared

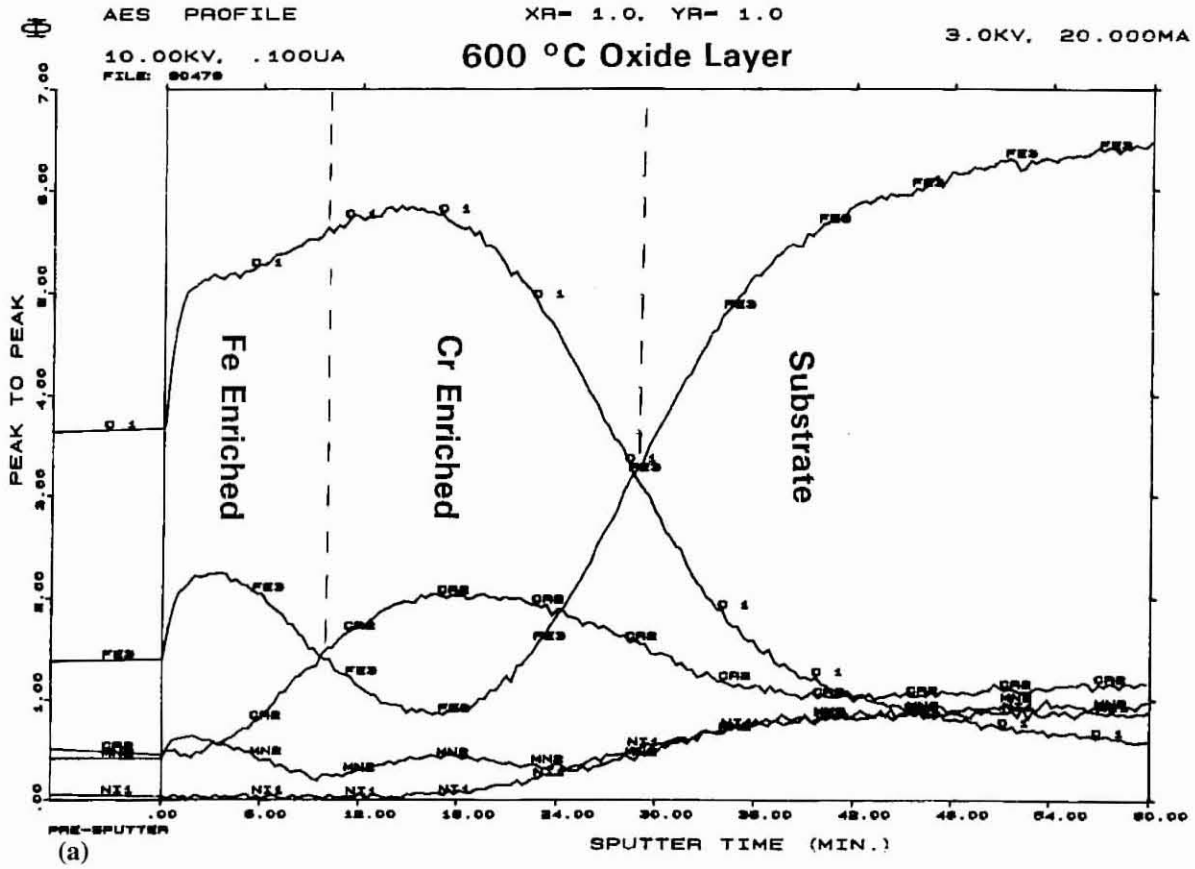

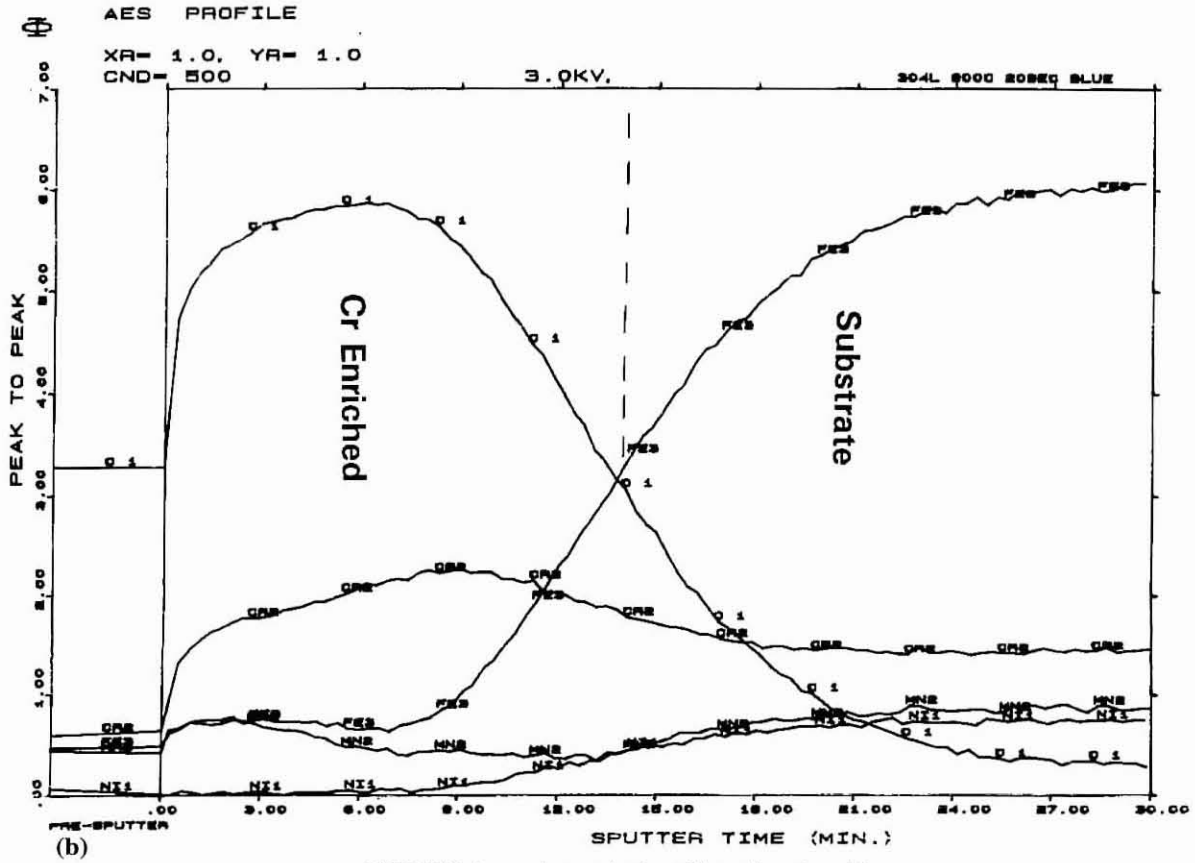

FIGURE 5. Auger-electron depth profiles on heat-tint oxides
(a) Specimen heated to 580 °C, with an iron-rich outer surface and a chromium-rich oxide layer below it
(b) Specimen heated to 880 °C, with a chromium-rich oxide

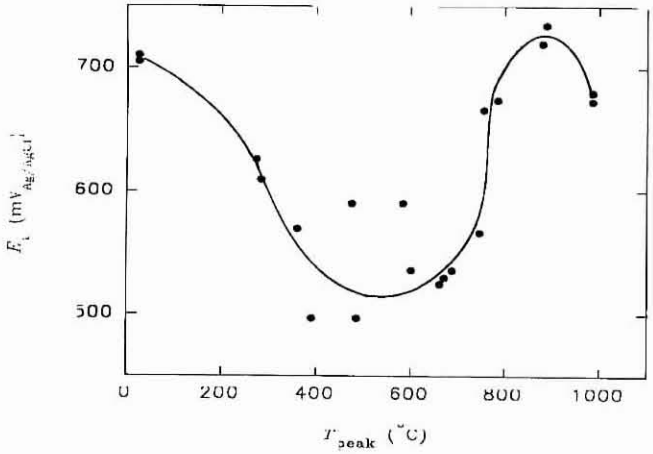

FIGURE 6. Breakdown potentials of type 304 specimens heated in air for 20 seconds to different peak temperatures (tested in 3,5 per cent NaCl, adjusted to pH 1, at ambient temperature, potential sweep rate 1 mV/s)

with the passivated specimen, but that these pits grew to a much smaller size before repassivating – it should be noted that the magnification in Figure 7(b) is approximately six times that in Figures 7(a) and (c). The surface density of pits on the 880 °C specimen in Figure 7(c) is similar to that on the passivated specimen, but the edges of the pits are much more irregular. The differences in pit shape are probably associated with changes in the nature of the oxide film, which forms a cover over the metastably growing pits. After the pitting tests, the larger pits on the 880 °C specimen could be seen to be covered with blisters. These blisters presumably form when the oxide film is undermined by pit growth; this visual observation confirms the important role of the oxide film in the early (metastable) growth of corrosion pits.

The stability of the thermal oxide film in the pitting solution depends on the film composition. This is demonstrated by Figure 8, which compares the film compositions before and after the pitting test for an initially iron-rich film, Figure 8(a), and for an initially chromium-rich film, Figure 8(b). The film composition after the pitting test was determined on apparently unattacked regions between corrosion pits. It is clear from Figure 8 that the iron-rich film dissolves away during the pitting test, while the composition of the chromium-rich film does not change greatly. This effect was confirmed by visual observation: specimens covered with iron-rich films lost their tint after being exposed to the pitting solution, while the colour of the chromium-rich films was unchanged.

Welded Specimens

The transition, with temperature, in pit size and surface density that was observed for the simulated specimens (Figure 7) could also be seen on the surface of welded specimens. The photomontage of Figure 9 shows this transition for a specimen tested at the rapid scan rate of 5 mV/s. The transition in pit size and number was no longer observed on a specimen tested at the much lower scan rate of 0,1 mV/s (Figure 10): the distribution of pits was much more uniform across the specimen, except for a region close to the fused zone, which was not attacked at all. It appears plausible that the more uniform pit distribution at the lower scan rate results from dissolution of the iron-rich film before it reaches the potential range where metastable pits can form. At

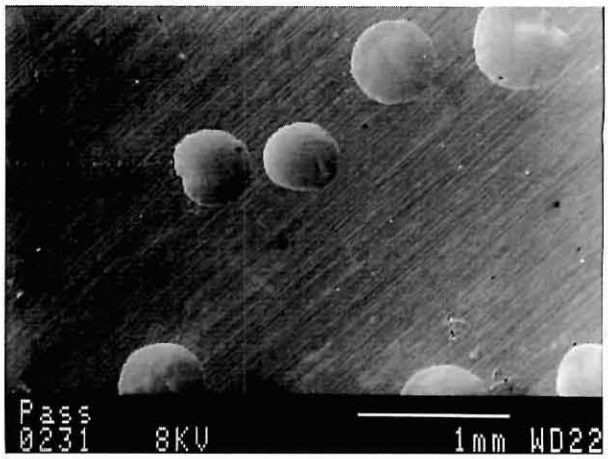

(a)

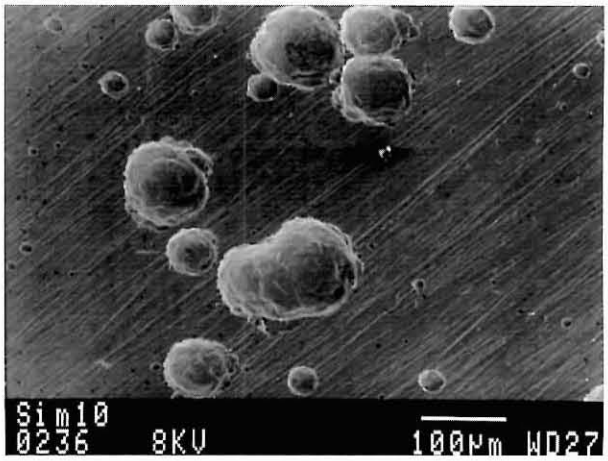

(b)

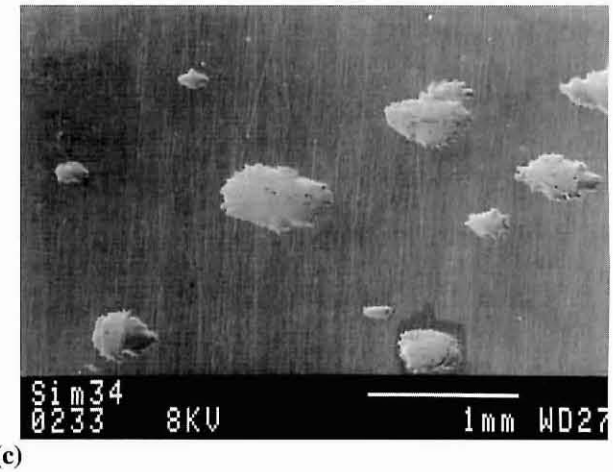

(c)

FIGURE 7. The effect of peak temperature during oxidation on the pit morphology during subsequent testing in 3,5 per cent NaCl at pH 1
(a) Passivated specimen
(b) Specimen heated to 380 °C
(c) Specimen heated to 880 °C

the lower scan rate, more time is available for the dissolution of the iron-rich film, which may explain the diminution of the effect of this film on the pitting behaviour of the metal. The unattacked region close to the fusion line was probably covered by a chromium-rich film, which is more stable in the acidic solution and so remains protective even at the lower scan rate.

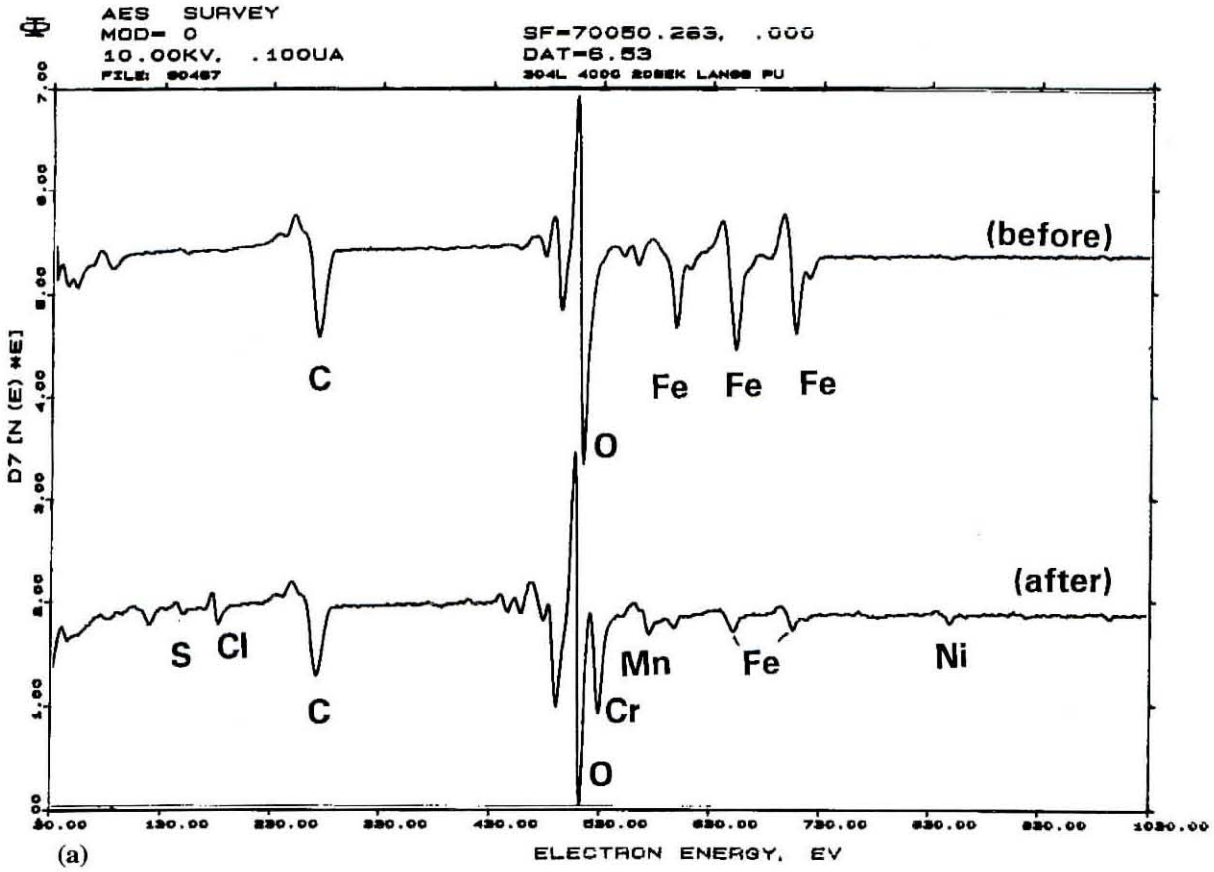

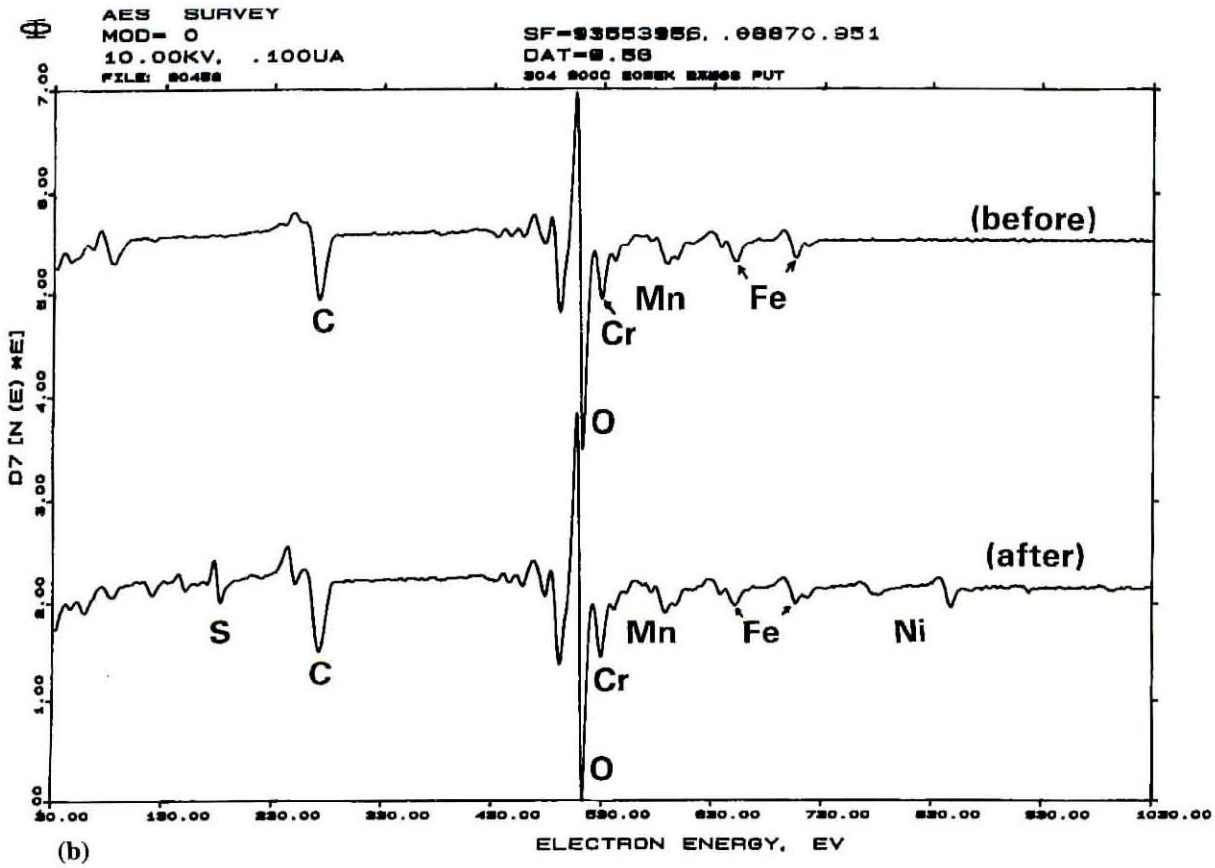

FIGURE 8. The effect of exposure of the heat-tinted specimens to 3,5 per cent NaCl at pH 1 on the composition of the outer region of the oxide film
(a) The composition of the iron-rich film on a specimen heated to 380 °C changes during exposure to the electrolyte, indicating that the film dissolves away
(b) The composition of the chromium-rich film on a specimen heated to 880 °C is largely unchanged after exposure to the electrolyte

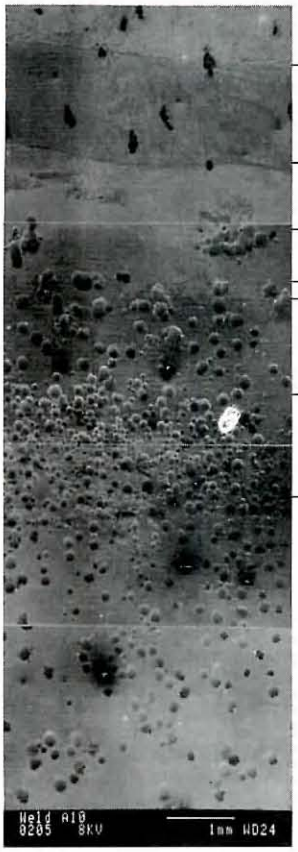

FIGURE 9. Photomontage of the appearance of a welded specimen after testing in 3,5 per cent NaCl at pH 1 and 5 mV/s. The heat-tint colours originally present on the surface are indicated

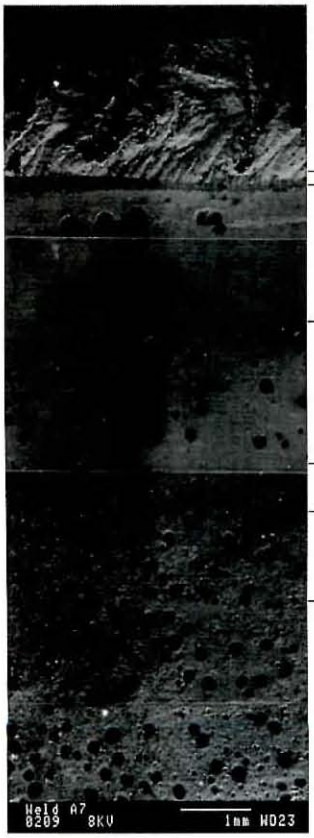

FIGURE 10. Photomontage of the appearance of a welded specimen after testing in 3,5 per cent NaCl at pH 1 and 0,1 mV/s. The heat-tint colours originally present on the surface are indicated

The surface analyses here refer to those regions of the weld that could be distinguished visually on the basis of the tints. Figure 11 shows the numerical designations given to the different tinted regions, together with the corresponding colours.

Weld	
Grey	5
Blue	4
Brown	3
Light Brown	2
Straw-coloured	1
No tint	0

4mm

FIGURE 11. Heat-tint regions on welded specimens, with the code numbers used to refer to each region

Surface analysis of the welded specimens revealed the same effects as were observed for the simulated specimens: iron-rich films at relatively low temperatures, chromium-rich at intermediate temperatures, and, again, iron-rich at high temperatures due to the volatilization of chromium. This is the case despite the presence of a shielding gas during the TIG welding operation. For the welded specimens, the gold marker layer allows the elucidation of the diffusion of iron and chromium at different temperatures. The oxide layer grows by cationic diffusion – thickening of the oxide takes place on top of the gold marker, which can be seen in Figure 12. Figure 12(a) gives the depth profile for the as-received metal (before welding, after the gold layer was added). After oxidation during welding, both chromium and iron are detected outside the gold marker. The depth profile in Figure 12(b) was determined at position 3 in Figure 11, where the outer oxide is enriched in chromium.

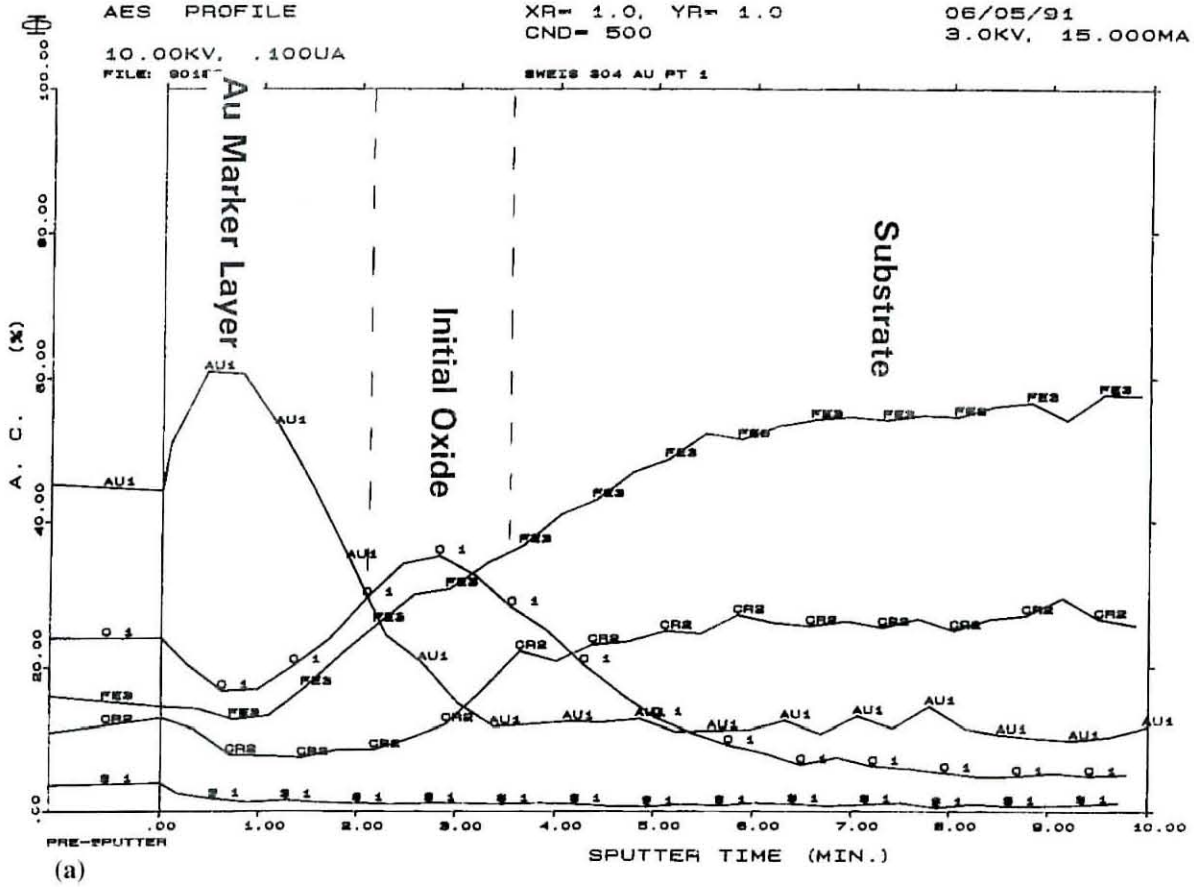

(a)

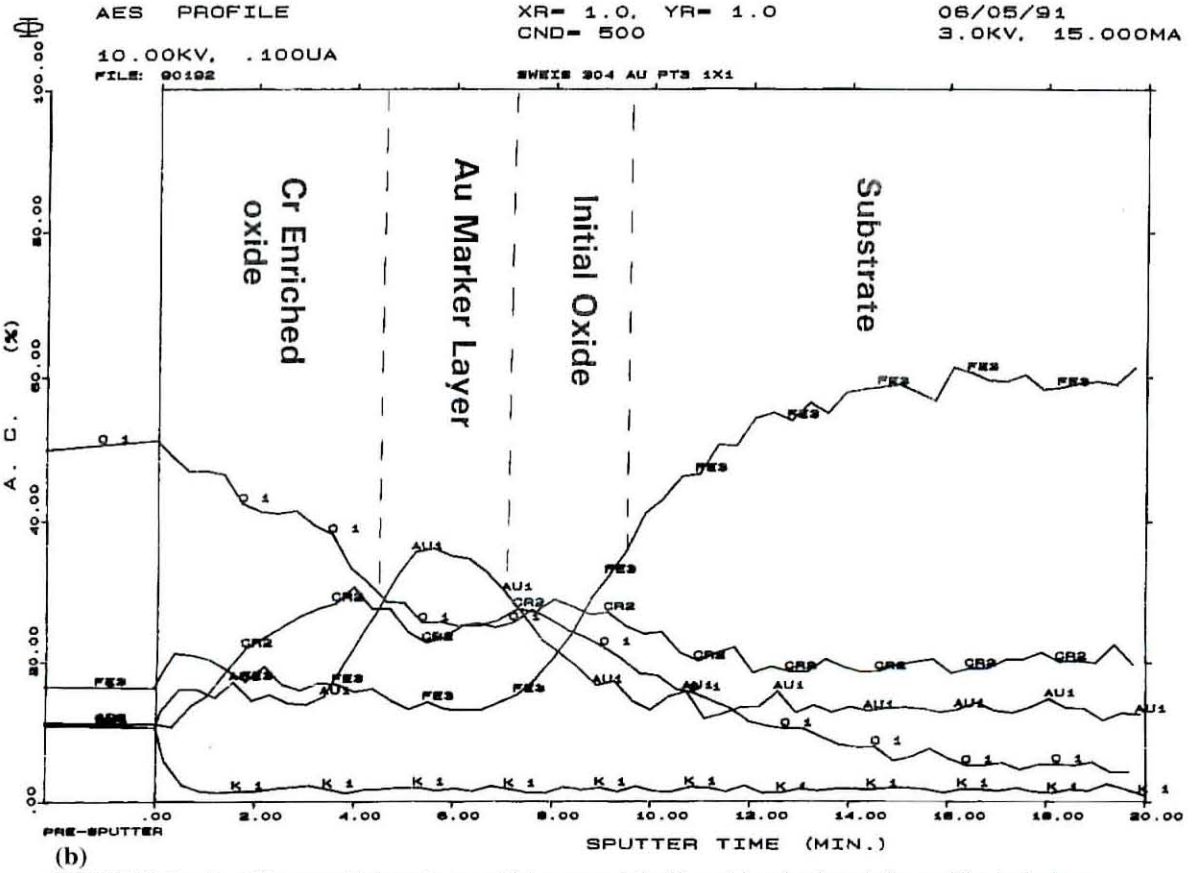

(b)

FIGURE 12. Depth profiles on welded specimens, which were coated with a gold marker layer before welding took place
(a) Metal before welding, showing the gold marker layer on top of the original passive film
(b) Depth profile of region 3 in Figure 11, showing the presence of the chromium-rich oxide that had formed on top of the gold marker layer during welding

The results for the compositions of the outer regions of the oxides found on the welded specimen are summarized in Figure 13, which plots the relative chromium and iron contents for the positions indicated in Figure 11. The results in Figure 13 can be seen to follow a similar trend to that for the simulated specimens (Figure 2): at relatively low temperatures (away from the fusion line, positions 1 and 2), the outer oxide has a low chromium content because of the more rapid diffusion of iron; at intermediate temperatures, chromium diffusion overtakes that of iron, with the result that the film is enriched in chromium (position 3); at the highest temperatures (close to the weld, positions 4 and 5), chromium is again lost from the film through volatilization.

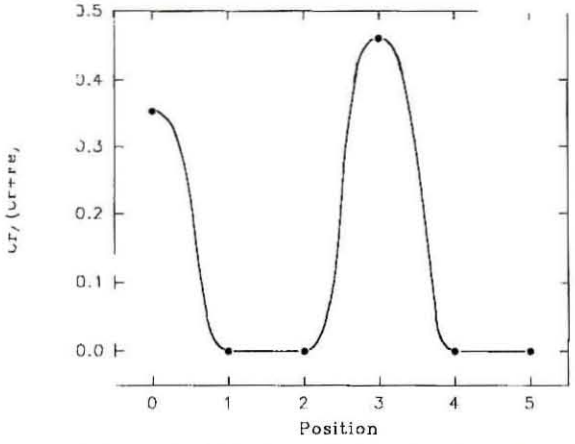

FIGURE 13. Relative chromium contents of the oxide films in the regions indicated in Figure 11, indicating that iron-rich oxide films form both at relatively low temperatures (positions 1 and 2, far from the weld) and at high temperatures (position 5, next to the weld), while a chromium-rich film forms at intermediate temperatures

No pitting could be detected (with a stereo-microscope) on those welded specimens which had been immersed, under open-circuit conditions, in the 3,5 per cent NaCl solution at 60 °C, even after 12 days' exposure. After this exposure, the only visible effect of the electrolyte on the metal was the removal of the heat tint. In contrast to this, pitting developed rapidly in the heat-tinted region when a specimen was immersed in the more aggressive pitting solution of 10 per cent $FeCl_3$ at ambient temperature. This is shown by Figure 14, which gives the potential profiles across the surface of the welded specimen at different times after the exposure of the specimen to the $FeCl_3$ solution. These potential profiles give the electrode potential of the welded specimen relative to a tin electrode that was scanned across the specimen surface. Anodic activity (e.g. a growing pit) is indicated by a more negative electrode potential. The very first scan (3 minutes after immersion) reveals the presence of propagating pits within the heat-tinted region on either side of the fusion line. At longer times, the pit to the left repassivates, while that to the right continues to propagate. Beyond 13 minutes, crevice corrosion developed between the edges of the specimen and the resin mount, precluding further measurements.

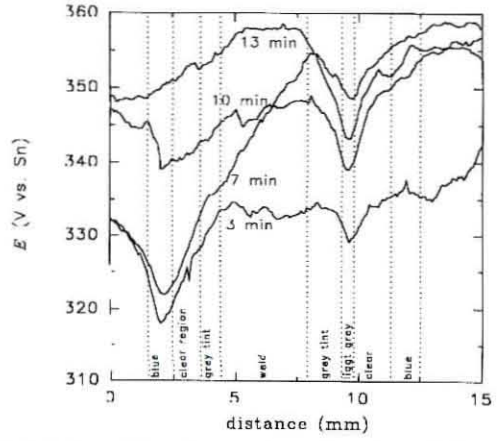

FIGURE 14. Potential profiles over the surface of a welded specimen immersed in 10 per cent $FeCl_3$, measured with a scanning reference electrode. The cathodic deflections in the potential profiles reveal the presence of pits in the heat-tinted region on either side of the weld

Discussion

The results for simulated weld specimens indicate that, under the experimental conditions considered here, iron-rich heat-tinted oxides are most deleterious to the pitting-corrosion resistance of type 304 stainless steel (Figures 2 and 6). This is contrary to a previously suggested mechanism for the detrimental effect of heat tint, namely that the chromium-depleted metal below chromium-rich oxides is more susceptible to pitting[1]. In the present investigation, the surfaces covered with chromium-rich oxides, in fact, exhibited the best resistance to pitting.

The detrimental effect of an iron-rich oxide film is not easily explained. The iron in the film is expected to be in the Fe^{3+} oxidation state and thus cannot undergo further oxidation. If it were possible to further oxidize the iron in the film, the accumulation of chlorides (by electromigration) at the surface of the metal could have served as a trigger to pit initiation. However, such a mechanism is apparently not possible here. One possible role of the iron-rich layer is to act as an ion-selective membrane, which allows the electromigration of chlorides from the electrolyte to the metal surface, but which hampers the outward diffusion of the chlorides away from the metal surface[12]. In this way, a large surface concentration of chloride ions may build up, triggering the many pit sites that were observed, Figure 7(b). Such a mechanism depends on the maintenance of an iron oxide film on the metal surface: if the iron oxide disappears (through chemical dissolution), the metal will behave like bulk metal, and no effect of the heat tint will be observed. This is a probable explanation of the difference in surface morphology of welded specimens tested at rapid and slow potential scan rates respectively (Figures 9 and 10): at the slow scan rate, the iron-rich film has dissolved before the pitting range is reached; at the more rapid scan rate, the metal reaches a potential range where it is susceptible to pitting while the iron-rich film is still present on the metal surface.

This difference in the importance of the heat-tint oxide, depending on the potential scan rate, suggests a possible explanation for the observation that heat-tint has a negative effect on pitting resistance only if the metal already operates at the limit of its corrosion resistance[1]. Such aggressive conditions imply a relatively positive corrosion potential, close to the pitting potential of the (untinted) base metal. Under these conditions, the heat-tinted region is rapidly brought into the potential range where the thermal oxide causes pitting; the exposure of the welded specimen to $FeCl_3$ is an example of this (Figure 14). This, it is suggested, is analogous to a rapid potential sweep rate.

On the other hand, if the potential remains below the pit-

ting range for a sufficiently long time, the heat tint can dissolve without any harmful effects: the metal effectively receives a pickling treatment *in situ*. The behaviour of the welded specimen during prolonged immersion in the 3,5 per cent NaCl solution at 60 °C is an example of this.

Extension of this work to alkaline environments, where the iron-rich film is expected to be much more stable, would be useful as a test of the validity of this idea.

The role of the iron-rich oxide film – to promote pit initiation – is not one that was envisaged at the outset of this work, where two possible roles were considered for oxide films: hampering pit initiation and stabilizing pit growth. It appears that the second envisaged effect of the oxide film – to sustain pit growth – is not centrally important under these conditions. This follows from the observation that, while the chromium-rich film of the specimen oxidized at 880 °C formed visible covers over the pits, allowing these pits to grow relatively large before repassivating, Figure 7(c), this specimen had a breakdown potential similar to that of the passivated specimen, Figure 6. In addition, the metastable pits on the specimen oxidized at 380 °C generally repassivated at much smaller radii (presumably because the iron-rich oxide is weaker); yet, in spite of this, this specimen had a much lower breakdown potential. Clearly, under these conditions, the number of metastable pits that form (rather than merely the stabilization of their growth) plays the central role. The importance of the number of metastable pits is apparent from the following relationship, which expresses the rate of formation of stable (destructive) pits as a function of the rate at which metastable pits nucleate[13]:

$$\Lambda = \lambda \exp(-\mu t_c). \qquad [1]$$

In equation [1], Λ is the rate at which stable pits form, λ is the rate at which metastable pits are nucleated, μ is the probability that a metastable pit will repassivate in an interval of unit time, and t_c is the critical age at which the metastable pit becomes stable. For the specimen oxidized at 380 °C, λ is much greater than it is for the passivated specimen (as indicated by the larger surface density of pits on the former specimen), but the smaller pit size suggests that μ is greater for the oxidized specimen (reflecting a greater change of repassivation due to a weaker oxide film). The more cathodic pitting potential of the oxidized specimen implies that it has a greater Λ at a given potential than the passivated specimen. From this, it appears that the increased rate of metastable pit nucleation (λ) plays a stronger role than the increased probability of repassivation (μ), at least in this case. The use of electrochemical noise measurements, rather than the comparatively crude expedient of pitting-potential determination, would be useful in an investigation of the validity of this argument.

Conclusion

A combined electrochemical and surface analytical study of heat tint on type 304 stainless steel suggests that iron-rich oxides can be detrimental to pitting-corrosion resistance. The deleterious effect of the iron-rich film is realized only if the metal reaches a potential in the region where it is susceptible to pitting before the film has dissolved chemically.

Acknowledgment

The authors are most grateful to Mr Pieter Pistorius for the preparation of the simulated weld specimens.

References

1. Kearns, J.R., and Moller, G.E. (1991). Optimizing the corrosion resistance of welded austenitic stainless alloys. Paper 182, Corrosion '91. NACE, Houston, (Texas).
2. Stockert, L., and Böhni, H. (1989). Susceptibility to crevice corrosion and metastable pitting of stainless steels. *Mater. Sci. Forum*, 44 and 45, pp. 313-327.
3. Isaacs, H.S. (1974). Potential scanning of stainless steel during pitting corrosion. In *Localized corrosion,* B.F. Brown, J. Kruger, and R.W. Staehle (eds.). NACE, Houston (Texas). pp. 158-166.
4. Gaudet, G.T., Mo, W.T., Hatton, T.A., Tester, J.W., Tilly, J., Isaacs, H.S., and Newman, R.C. (1986). Mass transfer and electrochemical kinetic interactions in localized pitting corrosion. *AIChE Journal,* 32, pp. 949-958.
5. Isaacs, H.S., and Kissel, G. (1972). Surface preparation and pit propagation in stainless steels. *J. Electrochem. Soc.,* 119, pp. 1628-1632.
6. Asami, K., and Hashimoto, K. (1979). An X-ray photoelectron spectroscopic study of surface treatments of stainless steels. *Corros. Sci.,* 19, pp. 1007-1017.
7. Hultquist, G., and Leygraf, C. (1981). Selective oxidation of a ferritic stainless steel and its influence on resistance to crevice corrosion initiation. *Corros. Sci.,* 21, pp. 401-408.
8. Isaacs, H.S., and Vyas, B. (1981). Scanning reference electrode techniques in localized corrosion. In *Electrochemical corrosion testing* (ASTM STP 727), F. Mansfield and U. Bertocci (eds.), Philadelphia, American Society for Testing and Materials. pp. 3-33.
9. Tuck, C.D.S. (1983). The use of micro-electrodes in the study of localized corrosion in aluminium alloys. *Corros. Sci.,* 30, pp. 379-389.
10. Hultquist, G., and Leygraf, C. (1980). Surface composition of a type 316 stainless steel related to crevice corrosion. *Corrosion,* 36, pp. 126-129.
11. Kofstad, P. (1984). Chapt. 1. In *High temperature materials corrosion in coal gasification atmospheres,* J.F. Norton (ed.). Amsterdam, Elsevier Publishers, pp. 1-57.
12. Newman, R.C. Personal communication.
13. Williams, D.E., Westcott, C., and Fleischmann, M. (1985). Stochastic models of pitting corrosion of stainless steels. I. Modelling of the initiation and growth of pits at constant potential. *J. Electrochem. Soc.,* 132, pp. 1796-1804.